

International Conference on Space Optics—ICSO 2022

Dubrovnik, Croatia

3–7 October 2022

Edited by Kyriaki Minoglou, Nikos Karafolas, and Bruno Cugny,



ALTIUS Instrument: A study of scattering effects



ALTIUS Instrument: A study of scattering effects

J. Moreno-Ventas^{a/b}, W. Moelans^c, A. Mazzoli^d, L. Aballea^c, P. Blain^d, E. Mazy^d, L. Clermont^d, N. Saillen^a, L. Montrone^a, M. Francois^a

^aEuropean Space Agency ESTEC, Noordwijk, Netherlands, ^bATG for European Space Agency, Noordwijk, Netherlands, ^cOIP Sensor Systems N.V. Oudenaarde, Belgium, ^dCentre Spatial de Liège, Université de Liège, Belgium

ABSTRACT

ALTIUS is the next ESA limb-sounding mission for monitoring of stratospheric ozone at high vertical resolution and of NO_x molecules and aerosols. With a platform based on the PROBA-NEXT concept flying in a Sun-Synchronous orbit, the data provided by the ALTIUS Mission will support the scientific community addressing key questions related to atmospheric chemistry composition and climate changes. The ALTIUS Instrument features wavelength-tuning capabilities in the UV (250-355nm), VIS (440-675 nm) and NIR (600-1020) bands using a Fabry-Perot interferometer (FPI) stack in the UV band and an Acousto-Optic Tunable Filter technologies (AOTF) in the VIS and NIR bands. This Instrument topology allows ALTIUS to perform 2D imaging with high resolution in the vertical profile of the Earth limb. The optical layout of 2D imagers, characterized by a more extensive field of view (FOV), makes them more susceptible to stray light issues in comparison to more conventional optical designs such as grating systems. These particular design aspects in combination with the use of novel technologies (FPI's and AOTF's) and the irradiance distribution of the observed bright limb scenes makes the stray light prediction very interesting and complex. An accurate modelling of scatter contributors involving optical and mechanical surfaces is, therefore, required.

Due to the cost-effective model philosophy applied for the ALTIUS Instrument, no hardware model is available for stray light correlation purposes prior to the Instrument Proto-flight. Hence, a study was performed to benchmark the stray light analyses results obtained with Optic Studio with the ones obtained with FRED.

This paper provides a description of the optical modelling features of the ALTIUS Instrument with specific attention to the novel optical devices, AOTF and FPI stack. It also addresses the particularities and differences observed when modelling the Instrument using two different commercial optical design suites. A comparison of scattered stray light computations for the ALTIUS Instrument ran in OpticStudio and FRED is also presented highlighting reflections on modelling approach and used mathematical models, with an outlook on consistency at L1. Finally, lessons learned from this exercise are presented along with the conclusions and plans for future work.

Keywords: Stray light, PSF, Analysis, Limb-sounder, Benchmarking; OpticStudio, FRED

1. INTRODUCTION

The ALTIUS mission, currently under development as an element of ESA Earthwatch Programme, is integrating a payload meant to perform imaging of the Earth limb with a high vertical resolution over an extended wavelength range from the UV to the near infrared with a moderate spectral resolution.

The innovative approach defined for the ALTIUS payload by the scientists is focusing on the possibility to perform direct 2D capture of the Earth limb vertical profile in one single image, generating the spectral datacube of the atmosphere by scanning wavelengths rather than spatial scanning. This approach, deviating from other and more classic limb sounder architectures, is presenting the advantage of a very accurate strict spatial co-registration of a complete atmospheric column. Nevertheless, this scientifically valuable approach is also generating several challenges for an optical payload to be designed. Beside the selection of the spectral filter technology, the optical design of the instrument shall be developed on a different approach than the traditional grating spectrometer/ imaging relay optics/scanner mechanism often used. Additionally, the challenge of this kind of design appears clearly in the stray light aspects considering the strong vertical irradiance distribution variation of the observed scenes and the stray light rejection difficulties a 2D design can implement within its field of view. As similar dataproduct and stray light optimization is required for L2 products derivation in the

same way as for a classical design, it is critical to accurately understand the stray light generated by the instrument in order to develop appropriate data processing approaches. This paper will present an initial comparative study made between two different stray light analyses softwares in order to probe the robustness of the analyses made for the ALTIUS payload and identify possible worst case approach for the stray light correction based on modelling uncertainties. The hereby presented modeling has been focusing on the UV channel at 300 and 350nm and the VIS channel at 650nm, based on scientific priorities identified by the primary stray light requirements.

2. ALTIUS INSTRUMENT DESCRIPTION

2.1 General instrument design description

The ALTIUS instrument (currently under development by OIP NV) is meant to be integrated on top of a PROBA P200 platform developed by QinetiQ Space. The ALTIUS mission is planned for a nominal timeline of three years with a possibility of extension for two years. It will be launched as a co-passenger using the Vega C launcher.

Due to the limited allocations in volume and mass, the payload had to be developed under severe volume constrains while still ensuring the allocation of three different sub-instruments (also called channels), imaging respectively in the UV range between 250nm and 355nm, VIS range between 440nm and 675nm and NIR between 600 and 1020nm. The three channels are optically and electrically fully independent from each other. The three channels are stacked on top of each other on the same mechanical assembly, called Optical unit. Each channel is electrically controlled by an independent control electronics assembly, each three assembly being positioned along the optical unit as shown in Figure 1.

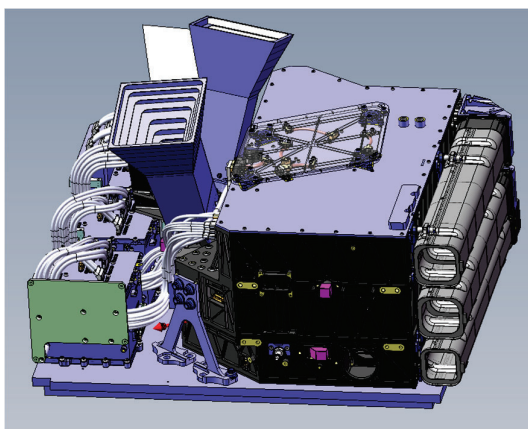


Figure 1. ALTIUS instrument optical unit and channels control units

The design of each of the three channels had to consider multiple observation modes required by the scientific community for the ALTIUS instrument as bright limb observations, solar and stellar occultation while ensuring for them the adequate radiometric, spectral and geometric performances. The main requirements on spatial performances and spectral sampling which shall be achieved by the payload are indicated in the Table 1 below.

Table 1. Main parameters guiding the optical design of the three channels

Requirements	Value
Minimum spatial sampling of the atmosphere projected at the tangent of the earth	Dx:20 km mandatory 1 km goal Dy:1 km mandatory 0.5 km goal
Spatial extension of the scene to be covered projected at the tangent of the earth	100 km
Minimum IFOV of a pixel	0.2 mrad
Spectral resolution	
- UV	Better than 2.5 nm
- VIS	Better than 10 nm
- NIR	Better than 10 nm

Based on an extensive feasibility study performed in the payload development phase B, backed up by breadboarding activities, spectral filters allowing a direct 2D spatial imaging in the relevant wavelength domain were selected for each of the channels. As such, the UV channel is based on Fabry-Perot technology; while the VIS and NIR channels integrate an Acousto-Optical Tunable filters (AOTFs) which has been identified as the best candidate based on the scientific requirements.

From a general standpoint, each channel is based on a reflective optical design organized over a unique layout:

- A front periscope mirror allowing fine co-alignment of the different Instrument Lines Of Sight (LOS's), protected from out of field stray light through use of a long front baffle, is collecting the light towards the instrument
- A succession of a Front End Optics (FEO), spectral filter and Back End Optics (BEO) Module that forms an image of the selected spectral band in the observed scene onto the detector;
- The Focal Plane Assembly which collects the generated photons of the vertical profile of the scene and transfers them into a digital image.

Considering technical and programmatic optimization of the payload development, the design of each channel is strongly focused on reusing the same subassemblies. Reusability has been leading to use of a quasi-identical optical design between the VIS and NIR channels. This is also for instance the case for the focal plane assembly, which is identically based on the CIS115 sensor from Te2V [1] on each channel. A detailed description of the payload and technologies onboard was already reported in [2] and the reader can also refer to [3] presented in this same conference and showing an overview of the current development status and challenges.

2.2 VIS and NIR channels opto-mechanical design

The VIS and NIR channels of the ALTIUS are almost identical from an optical design point of view. The design is presented in Figure 2.

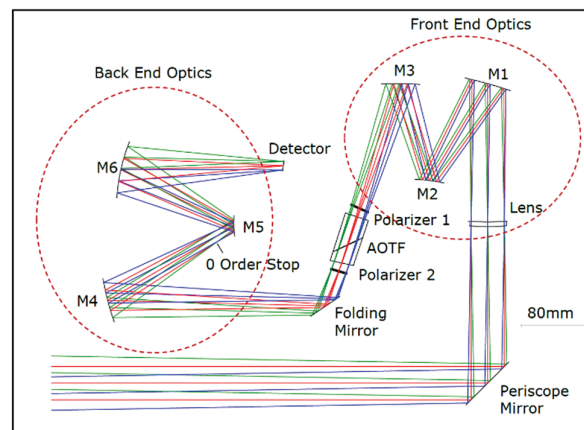


Figure 2. VIS channel optical design concept

In these two channels, the front end optics (FEO) is a telecentric objective composed of three mirrors integrated on a single mechanical structure. Its role is to match the AOTF aperture and acceptance angle while correcting the chromatic aberrations induced by the AOTF crystal. The FEO is generating an intermediate image of the scene few mm behind the AOTF crystal.

The AOTF is the spectral filter allowing a versatile selection of the wavelength to be imaged by the camera. The detailed AOTF acousto-optics interaction theoretical baseline is very well known and documented, for instance in [3]. From a high level standpoint, an acoustic wave, generated through a vibrating piezo actuator, propagates in a large high purity birefringent (TeO₂ for most VIS/NIR applications) crystal and defines a phase grating whose pitch is defined by the frequency of the wave. This phase grating interacts with the incoming beam generating a diffraction effect between a first diffracted order, containing the waveband of interest and a zero order which contains the undiffracted light. The central wavelength of the first diffracted order is defined by the frequency of the selected acoustic wave. The light from the first diffracted order intermediate image is then collected by a second TMA, called Back End Optics (BEO) which is a relay

towards the detector. The magnification of the BEO is then determined by the dimensions of the image projected onto the sensor chip.

Table 2. VIS and NIR channels first order parameters defining the optical design

Parameter	Units	VIS	NIR
Design FOV	mrad	35 x 35	
Entrance Pupil Diameter	mm	Ø42 & 34.5x42	Ø42
AOTF useful aperture	mm	20 x 20	20 x 20
AOTF separation angle	°	4.3 to 4.9	4.9 to 5.3
used number of used detector pixels		1503 x 1503	

One of the first challenge designing using AOTF technology is to filter out the narrow waveband first diffracted order from the very intense zero order containing the rest of the continuum from the incoming scene light. Fortunately, the acousto-optic interaction in a birefringent material presents some properties to ease the design:

- The AO interaction rotates the polarization of the first order diffracted light by $\pi/2$ with respect to polarization of the incident light while the zero order polarization state is left identical. As such it appears possible to perform a first stage of zero order reduction by using cross oriented polarizers in the front and back of the AOTF crystal.
 - In ALTIUS this is done through the use of double wiregrid polarizers presenting a very high rejection ratio (more than 10^{-6}). The zero order is therefore for a large part reflected back towards the entrance of the instrument.
 - One polarizer consists of two fused silica disks in front of each other with a dense grids of aluminum wires applied by lithography on each disk internal surface. The external surfaces are anti-reflection coated while the orientation of the wires of each disk is adjusted with a high accuracy.
- Due to the design of the crystal, the first diffracted order is exiting the AOTF at a different angle than the zero order. A careful mechanical design is therefore allowing to discriminate between the two orders:
 - The front lens in the FEO is integrating first a black mask made from Acktar “black magic”; which is adapting the design entrance pupil and incident light FOV to the separation angle between the zero and first diffracted order of the AOTF used. This mask ensures that a physical separation is feasible between the two orders.
 - The zero order being physically separated from the first order propagation path, it appears feasible to block it further in the optical path through use of a beam stop. In ALTIUS this is implemented in the back end optical module with a stop integrated in the TMA as shown in Figure 3.

The combination of these techniques is allowing a significant rejection of the zero order itself. Nevertheless this approach cannot suppress possible reflections and ghosts from the zero order on the refractive elements to find their way towards the detector.

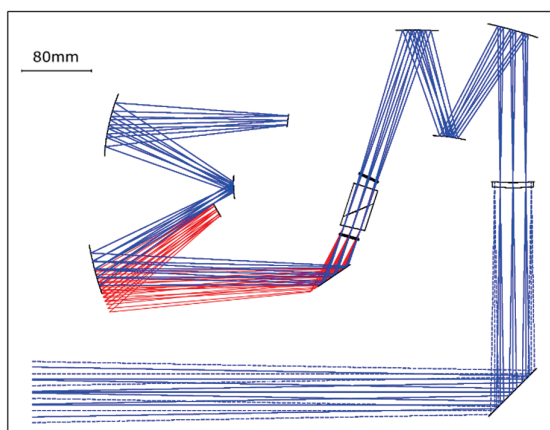


Figure 3. Zero order blocking method illustrated using a beam stop (red zero order, blue first diffracted order)

2.3 UV channel opto-mechanical design

In the UV channel, the optical design is quite different from the VIS and NIR channels. The spectral filter is based on a stack of four active Fabry-Perot interferometers. Each Fabry-Perot used for the ALTIUS mission is based on a dielectric-coated fused silica mirror pair connected together using piezo actuators with air gaps ranging between 400nm and 1000nm. Coating design of each mirror pair is tailored to ensure that the four FPI can select a narrow wavelength band in a continuous way between 250nm and 355nm. The main driver for the optical design is the limited étendue of the FPI, driven by the limitation of the mirrors clear aperture where the required parallelism could be guaranteed to achieve the required spectral performance. A maximum clear aperture of 12 mm has been identified as feasible, thus requiring for the stellar occultation SNR achievement to design a magnifier system and a line of sight changing mechanism. The optical layout is then split in two optical paths, one for bright limb and one stellar occultation as shown in Figure 4.

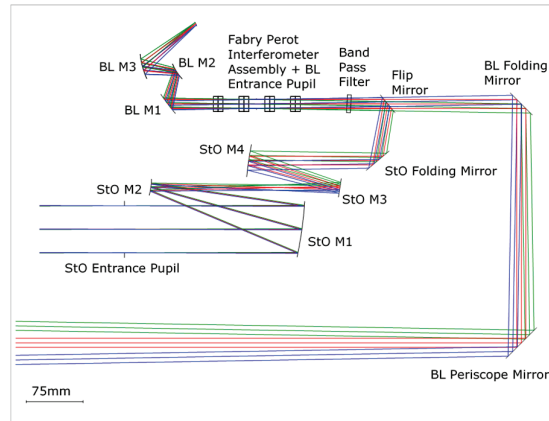


Figure 4. UV channel optical design

Considering the FPI stack to be mostly transparent in the visible range, the visible spectral rejection is done thanks to the use of a low pass filter coating applied on each mirror combined with a bandpass filter applied on a fused silica substrate. The main parameters of the UV optical design are identified in Table 3 below:

Table 3. UV channels first order parameters defining the optical design

Parameter	Units	Value Bright Limb	Value Stellar Occ.
Field of View	mrad	34 x 34	6.3 x 6.3
Entrance Pupil Diameter	mm	12	62
total focal length	mm	106	568
StO optics magnification	mm	-	5.38
intermediate image size	mm	-	7.1 x 7.1
image size	mm	3.591 x 3.591	3.591 x 3.591

3. STRAY LIGHT CRITICALITIES FOR ALTIUS

3.1 Scenes and requirements

The scenes to be observed for the ALTIUS mission are defined by the scientists based on the modelling of the atmospheric transfer function using MODTRAN. These scenes, in particular in the bright limb period of the orbit are characterized by an extremely strong dynamic range from the bottom of the atmosphere to the top of the 100km scene observed. This distribution is shown very clearly in Figure 5, which contains all required wavelength of observation for the instrument.

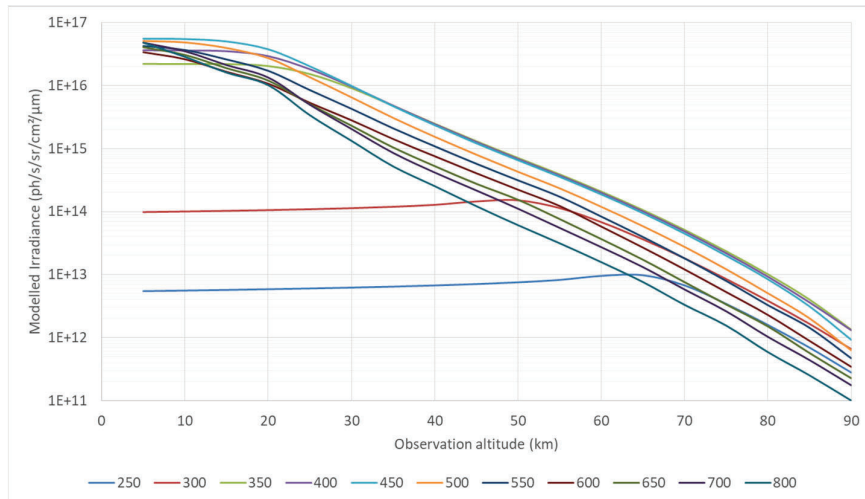


Figure 5. Irradiance of the scene modelled by the scientists as a requirement for the ALTIUS radiometric performances

Considering the above-mentioned scenes the scientists have been defining rather challenging radiometric requirements in terms of signal to noise ratio for the instrument.

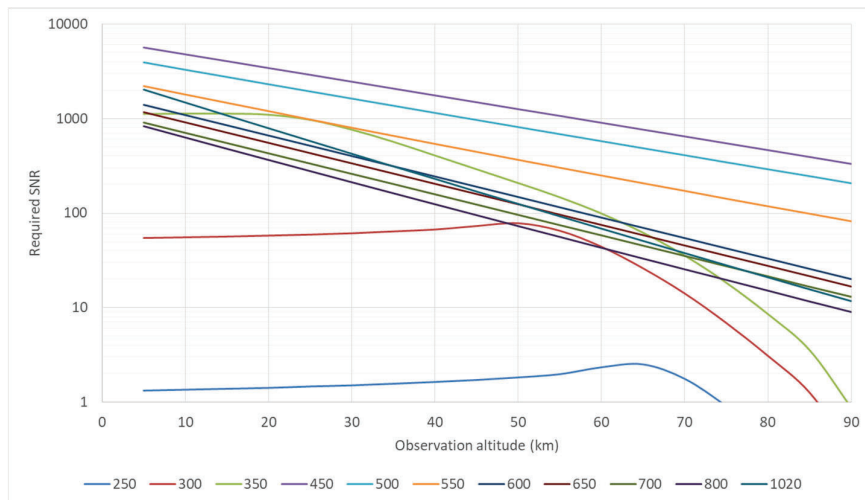


Figure 6. Required signal to noise ratio as a function of the images altitude for the scene specified in Figure 5

Based on the required collected signal they have also defined a stray light requirement specified in terms of stray light rejection based on a ratio between the stray light and the available signal. This requirement is basically allowing the stray light to be a maximum of 3x the noise from the detection chain.

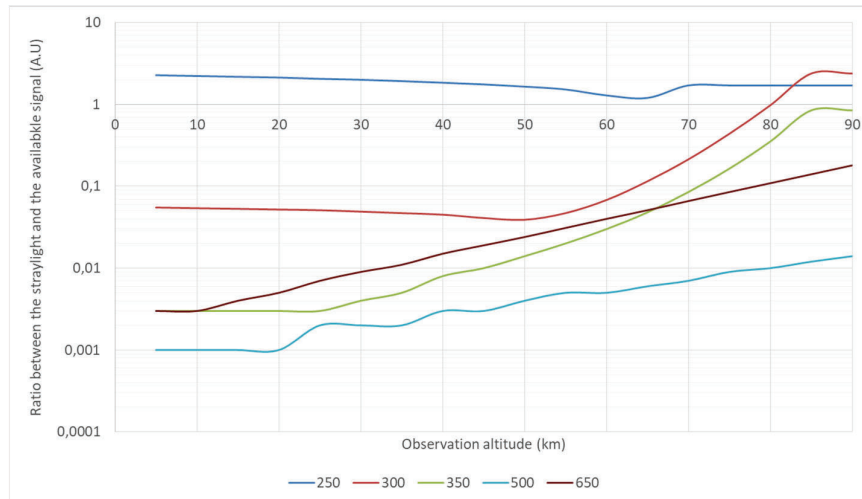


Figure 7. Stray light to signal ratio required as a function of the observation altitude

3.2 Specific sensitivities and way forward

Considering the stray light requirement and the irradiance distribution for the scene is already representing a significant challenge for the ALTIUS instrument concept as the stray light rejection shall occur in field. In such configuration there is little parameters to play with to optimize the optical design for in field stray light reduction; the scattering and the ghosting.

The scattering effect induced by each optical element plays an important role in the end to end achievable performances. The first optimization parameter in this matter is the optimization of the number of optical surfaces allowing still the design of each channel to fit within the allocated volume. The second optimization parameter is the selected technology for the manufacturing of the mirrors and refractive elements. Refractive optical elements are based on polished fused silica substrate. For reflective optical elements, selected approach is based on the reduction of the micro roughness of each unique optical surface. Considering the all-aluminum approach for the ALTIUS design, it has been decided to go for polished nickel plated mirrors which would satisfy the target of reach a surface roughness ≤ 1 nm RMS in an extended frequency range from 1.5mm^{-1} to 2000mm^{-1} .

To support the stray light analyses, achievable performances for polished nickel plated mirrors have been validated through prototypes development. The bidirectional scattering distribution function (BSDF) has been measured at 633nm on samples and an ABg function has been fitted to the measurement, shown in Figure 8. For the mirrors, two models, one for small angle scattering (PV-EVO SAS) and one for large angle scattering (PV-EVO LAS) are combined for the roughness scattering simulation. The parameters of these models are given in Table 4.

Other ABg models are defined for the scattering of the refractive surfaces, one for the UV channel and one for the VIS channel. A unique model is used for the reflective and refractive surfaces as well as the detector for the scattering from particulate contamination [4]. The Mie scattering model for particulate contamination with a slope of 0.383 and a cleanliness level of 361 corresponding to an obscuration of 600ppm has been simulated with ABg functions, see Figure 9.

Table 4. Parameters of the ABg models for the fitted BSDF of polished nickel plated mirrors

Name	λ [nm]	A	B	g
PV-EVO - SAS	633	2.555E-9	1.797E-12	3.92214
PV-EVO - LAS	633	8.055E-5	6.643E-4	1.10956

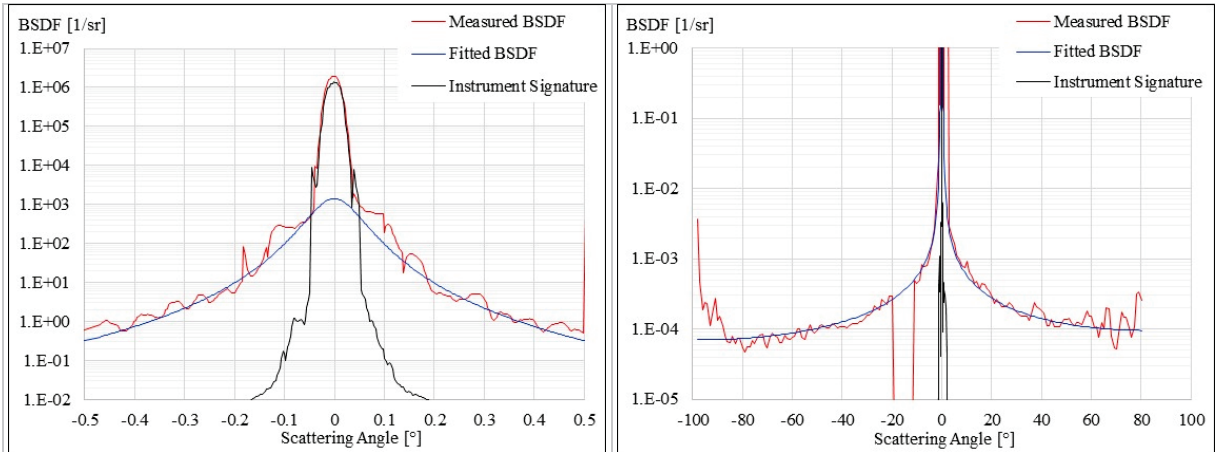


Figure 8. Example of BSDf measured on polished nickel plated mirrors together with the fitted BSDf and the signature of the measurement equipment.

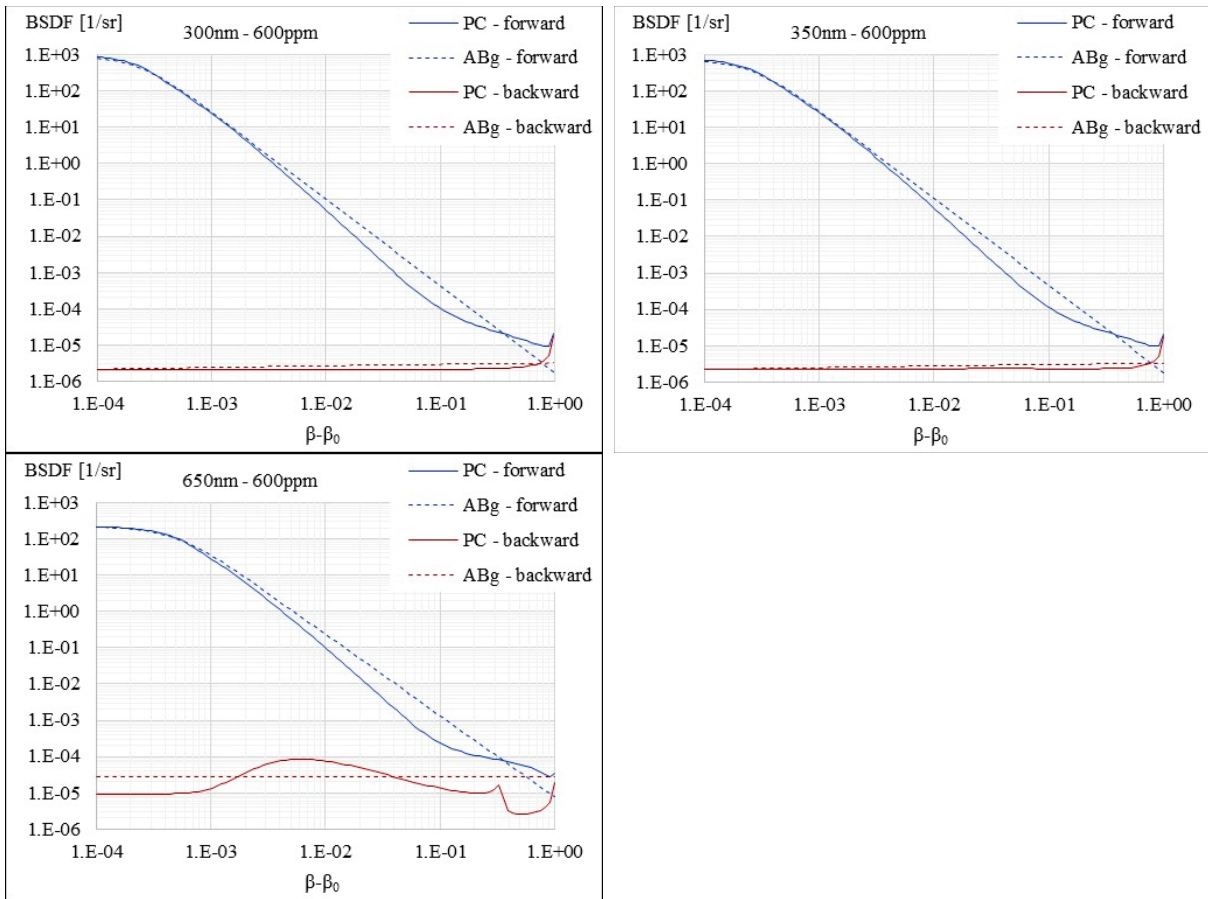


Figure 9. ABg curves used to simulate particulate contamination

Optimization of ghosts has been performed by scrutinizing the respective orientation of all surfaces which would contribute, namely the detectors, FPIs, bandpass filters, AOTFs and wire grid polarizers. Their respective orientations have been selected such that, if there is ghosting occurring it shall preferably lead to a ghosts which originates from the same altitude within the scene, to avoid cross contamination and ease the deconvolution methodology on ground. The design for each channel has therefore been optimized considering simple best engineering practices, namely:

- The FEO front lens curvatures have been defined to increase the defocus of ghosts originating from the lens,
- The tilt angles of the front and back AOTF polarizers are tuned such that the ghosts generated by first and zero order reaching the detector are getting reduced,
- The design is optimized for a detector which is tilted with respect to the incident rays so that rays reflected on the sensor don't hit the mirrors,
- The orientation of each refractive surface within the UV channel has been selected such that ghosts are generated outside the FOV of the instrument and originate from the same altitude than the scene.

Beside the infield stray light another challenge to be tackled for the ALTIUS is the near out of field stray light. Indeed the ALTIUS instrument shall be managing an irradiance profile coming from the earth, just below the field of view which could range between 1000 and 500 times the irradiance from the brightest part of the scene. This extremely bright near out of field elements could have a significant impact onto the stray light within the field.

3.3 Benchmarking needs

A comparison between the results obtained for the stray light values using two different optical software suites is considered necessary and of great added value for the ALTIUS stray light analysis. In the study, the softwares OpticStudio® and FRED® are used.

The goal of the study is to assess the stray light performance of the UV and VIS channels. For that, the PSFs for different wavelengths and fields are generated and compared using a mathematical criterion that quantitatively measures how different they are. Based on the results from this criterion and also in the overall distribution of the stray light irradiance, their differences and the validity of the models will be assessed. Additionally, the stray light irradiance distribution for the Bright Limb scene is also calculated for different wavelengths and the pixel stray light values compared to the requirements.

The UV and VIS optical and mechanical parts are modelled in both softwares, together with the sources, coatings, and scatter models. For the purpose of the study and in order to keep computation times reasonable, a simplified detector of 501x501 pixels with 21 microns pitch is used. Details and particularities on the modelling of the different parts are described here below.

4. STRAY LIGHT MODELLING

4.1 Scattering model

The initial finding comparing FRED and OpticStudio is coming from the way the scattering effects can be modelled. In OS, the only built-in scattering model to model scattering from polished optical surface is the ABg model.

$$\text{BSDF}(\beta-\beta_0) = \frac{A}{B+|\beta-\beta_0|^g} \quad (1)$$

β_0 and β are the projections of the specular and scattered ray vectors down to the surface.

The ABg model in OpticStudio has the limitation that the B parameter cannot scale below 1E-12. With the PV-EVO SAS function this limit is reached for wavelengths below 545nm. To overcome this the PV-EVO SAS function was modified slightly. The ABg models used to simulate surface roughness are given in Table 5. The full mirror scattering function, SAS + LAS, together with the PV-EVO function is shown in Figure 10 on the left.

Table 5. Parameters of the ABg models used in the OpticStudio model to simulate surface roughness

Name	λ [nm]	A	B	g
Mirror - SAS	633	4.11E-08	2.61E-11	3.47
Mirror - LAS	633	8.055E-5	6.643E-4	1.10956
Fused Silica VIS	633	2.55311E-6	6.38278E-5	2.3
Fused Silica UV	633	5.51068E-7	5.08026E-4	2.3

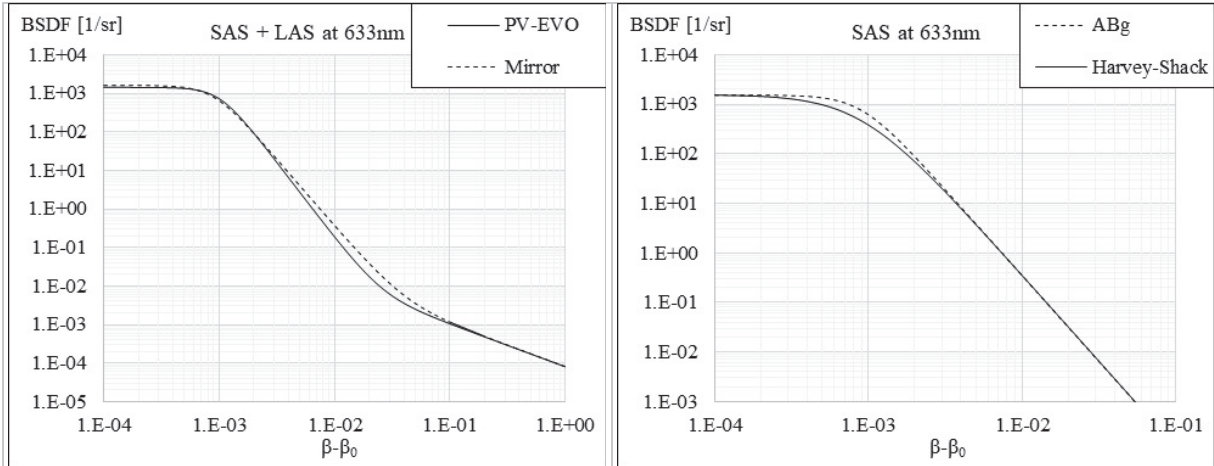


Figure 10. Comparison of PV-EVO BSDL and BSDL used in OpticStudio for mirror roughness (left) and comparison between ABg and Harvey-Shack model (right)

As the original stray light model was built in OpticStudio, scattering ABg functions derived from the roughness measurements of the different optical element presented in §3.2 were used.

Initially and in order to maintain consistency between the two models the ABg approach was also kept for the integration in FRED. Nevertheless initial investigation on the model consistency in FRED revealed that the obtained Total Integrated Scattering (TIS) computed with FRED appears not correct for models presenting a very sharp BSDL which is the case for the SAS mirror roughness scattering function. As an example, the scattering model for the ALTIUS mirrors prototypes has a TIS value obtained with OS as well as analytically of 3.2% at 300 nm, but the TIS computed with FRED for the same ABg model is 0.35%. This was attributed to the too high necessary sampling to perform the integration which is not supported in FRED.

Therefore it was necessary to come back with FRED to a Harvey-Shack (HS) model.

$$BSDL(\beta - \beta_0) = b \left(1 + \left(\frac{\beta - \beta_0}{L} \right)^2 \right)^{s/2} \quad (2)$$

The HS parameters have been obtained using the following conversion equations between ABg and HS model:

$$b = A/B \quad (3)$$

$$L = B^{1/g} \quad (4)$$

$$s = -g \quad (5)$$

Based on the conversion corresponding to the same ABg model the analysis of the TIS showed a value closer to the expected value but still slightly different (2.4%).

The ABg and HS parameters are given for a reference wavelength of 633 nm and a scaling with wavelength is performed to obtain the parameters for 300 and 350 nm for the UV design and 650 nm for the VIS design.

OpticStudio automatically scales the ABg function according to the following scaling laws:

$$A' = A \left(\frac{\lambda}{\lambda_{ref}} \right)^{g-4} \quad (6)$$

$$B' = B \left(\frac{\lambda}{\lambda_{ref}} \right)^g \quad (7)$$

$$g' = g \quad (8)$$

For the Harvey-Shack functions this translates to:

$$b' = b \left(\frac{\lambda_{ref}}{\lambda} \right)^4 \quad (9)$$

$$L' = L \left(\frac{\lambda}{\lambda_{ref}} \right) \quad (10)$$

$$s' = s \quad (11)$$

The models parameters are presented in Table 6. OpticStudio uses the ABg functions while in FRED the mirror SAS and the fused silica are replaced by Harvey-Shack functions. The ABg and Harvey-Shack models present small differences but their impact has been checked on the resulting PSFs and they were showed to be not significant for the final results.

Note that the backward particulate contamination (PC Backward in the table below) is not included in FRED because FRED does not allow negative g values.

Table 6. ABg & Harvey-Shack models used for the scattering of the mirrors

Name		ABg				Harvey-Shack		
		300nm	350nm	650nm		300nm	350nm	650nm
Mirror SAS	A	6.11E-08	5.63E-08	4.05E-08	b	31212.69	16847.83	1416.324
	B	1.92E-12	3.34E-12	2.86E-11	L	4.224E-04	4.93E-04	9.15E-04
	g	3.47	3.47	3.47	s	-3.47	-3.47	-3.47
Mirror LAS	A	6.97E-04	4.47E-04	7.46E-05				
	B	2.90E-04	3.44E-04	6.84E-04				
	g	1.10956	1.10956	1.10956				
Fused Silica UV/VIS	A	1.96E-06	1.51E-06	2.44E-06	b	2.15E-02	1.16E-02	3.60E-02
	B	9.12E-05	1.30E-04	6.78E-05	L	1.75E-02	2.05E-02	1.54E-02
	g	2.3	2.3	2.3	s	-2.3	-2.3	-2.3
PC Forward	A	1.72E-06	1.79E-06	7.55E-06				
	B	1.93E-09	2.52E-09	3.54E-08				
	g	2.4	2.4	2.25				
PC Backward	A	9.90E-06	1.02E-05	8.79E-05				
	B	2.14E+00	2.14E+00	2.14E+00				
	g	-0.1	-0.1	0				

4.2 Conservation of energy

Modelling the surface roughness and the particulate contamination requires that several scattering functions are applied to the surface. For the mirrors, for instance, four scattering functions must be added: SAS, LAS, the PC backward and the PC forward that is reflected on the mirror. In OpticStudio, ABg files can be added in two ways: relative and absolute. With the relative option the combined scattering function is the weighted average of the ABg functions, with the absolute option, the combined scattering function is the weighted sum. Obviously the ABg functions need to be added with the absolute option.

A simple test was performed on a 100% reflective flat surface with the combined ABg functions and it was found that the total power received by a hemispherical polar detector was larger than the power of the source. This is only the case with the absolute option. With the relative option the energy is conserved. As a workaround, scaled ABg functions were created with $A' = nA$ where n is the number of ABg files to be added and the scaled functions were added with the relative option.

4.3 Ray trace settings

Both FRED and OpticStudio have settings for dropping rays like minimum absolute and relative power and maximum number of intersections. According to the OpticStudio manual, the maximum number of generations of child rays split off from the parent ray is controlled by the maximum intersections per ray. This has been set arbitrarily to the maximum of 4000. FRED has a setting that has no equivalent in OpticStudio: ancestry level. This parameter directly limits the number of generations for specular and scattered rays. Considering the computation intensive aspect of the stray light analysis setting a number of ancestries optimizes the computation time as allowing to trace less rays in the source in FRED compared to OpticStudio. It also permits to reconstruct final results as a stack of different layers of paths while for OpticStudio the approach is more brute force. Nevertheless, this approach also requires the optical designer to know a priori what he is looking for to observe and induce the risk to “miss” significant effects in a first instance, risk prevented in the OpticStudio approach.

4.4 Modelling of the Components

The model was first built in OpticStudio. The mechanics is simulated with native OpticStudio objects. These objects were exported as a STEP file and imported in FRED. For this study the non-optical surfaces were defined as fully absorbing.

Coating on optical surfaces are defined with a general sampled coating using reflectance or transmittance values at the wavelengths of interest as a function of several incidence angle and for both polarization states s and p .

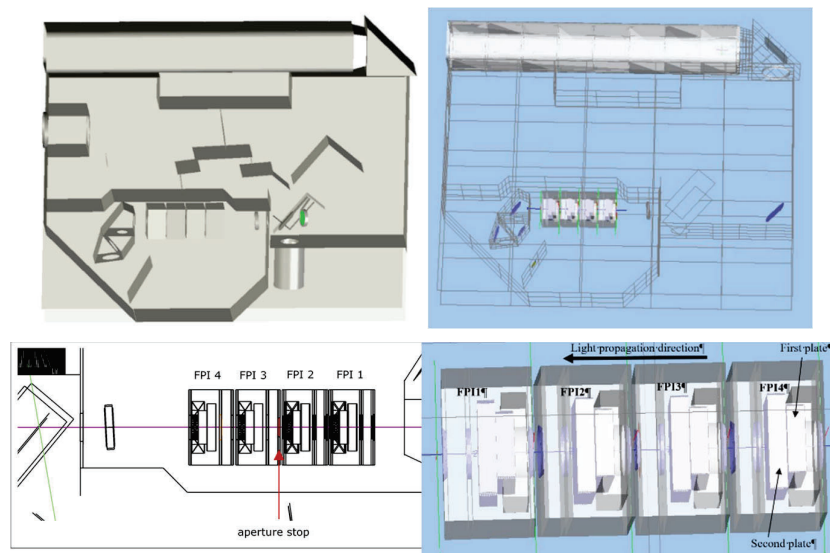


Figure 11. Imported mechanical element (Left: OpticStudio; Right: FRED) of the UV channel, close up of FPI's shown at the bottom.

The UV channel is relatively easy to model both in OpticStudio and FRED. The only unconventional components are the FPI's. The FPI's are modelled as two fused silica rectangular volumes. In OpticStudio they are in contact. FRED doesn't support two surfaces being positioned in the exact same position therefore there is an air space of 1µm between them. The transmission and reflection properties of the FPI are defined by means of a coating on the front face of the second plate. The front and back face of the first plate and the back face of the second plate all have a coating with 100% transmission. It shall be noted that in both models there is no integration nor consideration about the full spectral transfer function of the FPI units and or their respective constructive interference patterns. Therefore the analysis both in FRED and OpticStudio is excluding the spectral stray light which could originate from the spectral leakages due to imperfect coating design.

The VIS channel has two unconventional components that require some tricks to model: the wire grid polarizers and the AOTF.

The wire grid polarizers are double polarizers with the wire grids on the internal surfaces. They are modelled as two fused silica disk, 1mm thick, with a 0.1mm air space. Wire grid polarizers mainly reflect the rejected polarization. OpticStudio has a type of surface that is ideally suited to model this type of behavior: the Dual Brightness Enhancement Film (BEF) Surface. The Dual BEF Surface is a rectangular plane for which reflection and transmission in X and Y can be defined. FRED does not have this type of surface or coating therefore different models had to be made for X- and Y-polarized light.

In OpticStudio two Dual BEF Surfaces are placed inside the air space at 1µm from the fused silica disks. The outer surfaces of the disks have an anti-reflection coating with 99% transmission and 1% reflection, the inner surfaces have a coating with 100% transmission. The Dual BEF Surface has: reflection X 12.832%, reflection Y 99.998%, transmission X 87.168% and transmission Y 0.002%.

In FRED the polarizers are modelled with ordinary coatings on the faces of the fused silica disks and additional ideal polarizers and rotators. There are different models for the 1st order with an X-polarized source, the 0 order with an X-polarized source and the 0 order with a Y-polarized source. In first order with an X-polarized light source, everything is straight forward and the transmission and reflection values are the same as for the Dual BEF surface except for a small correction for the second polarizer that is rotated 3° round its normal to simulate alignment uncertainty.

To determine the transmission and polarization properties of each polarizer part in the zero order, an on-axis polarized point source was traced in OpticStudio and the power in front of, in the middle and behind each dual polarizer was recorded for X- and Y-polarized light separately. The results are given in Table 7.

Table 7. Flux in front, in the middle and behind each polarizers for a polarized source and a polarized detector, traced in OpticStudio with the Dual BEF models.

Source Polarization	X	X	Y	Y
Detector Polarization	X	Y	X	Y
In front of polarizer 1	9.77E+00	1.99E-05	1.42E-03	9.62E+00
In the middle of polarizer 1	8.43E+00	4.23E-05	4.85E-06	1.94E-04
Behind polarizer 1	7.27E+00	3.66E-05	4.27E-06	3.42E-09
In front of polarizer 2	7.09E+00	4.89E-02	4.16E-06	3.43E-08
In the middle of polarizer 2	2.02E-04	3.41E-02	1.24E-10	2.39E-08
Behind polarizer 2	2.00E-05	2.94E-02	1.34E-11	2.06E-08

In the zero order with an X-polarized light source, the first polarizer is the same as for the first order. After travelling through the AOTF a small part of the light is Y-polarized. The first part of the second polarizer will reflect almost all the X-polarized light but transmits most of the Y-polarized light. To simulate this a rotator is placed between the two parts of the second polarizer. With a Y-polarized source, a very small part of the light is X-polarized when it reaches the first polarizer. This part is transmitted by the first polarizer. After the first polarizer the light is mainly X-polarized and thus a rotator is placed after the second polarizing face. The complete model used in FRED is given in Table 8.

Table 8. Model of polarizers in FRED

	1 st order X-polarized source	0 order X-polarized source	0 order Y-polarized source
Polarizer 1 part 1 front face	T 99% - R 1%	T 99% - R 1%	T 99% - R 1%
Polarizer 1 part 1 back face	T 87.168% - R 12.832%	T 87.168% - R 12.832%	T 0.002% - R 99.998%
Polarizer 1 part 2 front face	T 87.168% - R 12.832%	T 87.168% - R 12.832%	T 2% - R 98%
	-	-	Rotator
	X-polarizer	X-polarizer	X-polarizer
Polarizer 1 part 2 back face	T 99% - R 1%	T 99% - R 1%	T 99% - R 1%
AOTF	Rotator	-	-
Polarizer 2 part 1 front face	T 99% - R 1%	T 99% - R 1%	T 99% - R 1%
Polarizer 2 part 1 back face	T 86.929% - R 13.071%	T 0.5% - R 99.5%	T 0.5% - R 99.5%
	-	Rotator	Rotator
Polarizer 2 part 2 front face	T 86.929% - R 13.071%	T 87.168% - R 12.832%	T 87.168% - R 12.832%
	Y-polarizer	Y-polarizer	Y-polarizer
Polarizer 2 part 2 back face	T 99% - R 1%	T 99% - R 1%	T 99% - R 1%

The AOTF is modelled similarly in OpticStudio and FRED. The AOTF is modelled in different parts. The AOTF material is birefringent TeO₂. The acoustic wave acts like a grating and is modelled as such. The groove spacing is chosen so that the diffracted ray has the correct angle after exiting the crystal. For a grating to function properly in both FRED and OpticStudio it needs to be immersed on both sides in non-birefringent material. In the used diffraction order, light entering the crystal is polarized perpendicular to the plane of diffraction, X-direction, and exits the crystal polarized parallel to the plane of diffraction, Y-direction. To simulate this a polarization rotator in the form of a Jones matrix is added near the grating. Because the grating normal is at a large angle θ with the incident rays, the Jones matrix doesn't have the conventional form. It was empirically derived that the Jones matrix has to be defined as follows:

$$\begin{aligned}
 A &= 0 & B &= -1/\cos\theta \\
 C &= 1/\cos\theta & D &= -\tan^2\theta
 \end{aligned}$$

There are two main differences between the AOTF models in FRED and OpticStudio:

- 1) In FRED it is not possible to put a coating on a birefringent surface therefore thin plan-parallel plates in non-birefringent TeO₂ were placed at the entrance and exit of the AOTF.
- 2) In OpticStudio there is no built-in way to model the diffraction efficiency as a function of the diffracted angle. The diffraction efficiency was modelled with a coating on a separate object inside the AOTF crystal. To make it easier to compare the results, the diffraction efficiency was also modelled with a coating on the grating in FRED.

The zero order is modelled in OpticStudio by setting the grating order to zero, changing the coating on the AOTF efficiency object to 100% and changing the Jones matrix to $A = D = 1$ and $B = C = 0$. In FRED, the grating and the Jones matrix are removed.

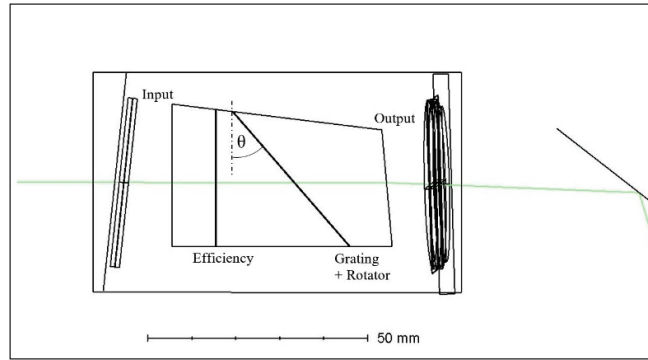


Figure 12. AOTF in OpticStudio

4.5 Modelling of the Scene

The characteristics of the sources are given by the geometry of the scene and by the optical characteristics of the instrument. ALTIUS will be observing the limb of the atmosphere from a 725km orbit, which gives an object distance of about 3000 kilometers.

The bright limb scene is modelled in OpticStudio with a set of extended sources of the type Source Two Angle. The infield that covers about 100km x 100km of the bright limb is modelled with 21 sources, 2.1° wide in the X-direction and 0.09572° wide in the Y-direction. The near out-of-field is modelled with a further 21 sources on both sides of the infield sources and one wide source at the bottom. Together the sources cover a field of view of ±6° in the horizontal direction and +1.005°/-6° in the vertical direction. The details of the sources are given in Table 9.

The spectral radiance L of the bright limb source is given in photons/s/sr/cm²/μm. The radiant power Φ in W of the sources is calculated as:

$$\Phi(\lambda) = L(\lambda, t) \cdot h \cdot c \cdot \frac{1}{\lambda} \cdot \text{FWHM}(\lambda) \cdot \Omega_{\text{source}} \cdot A_{\text{source}} \quad (12)$$

with:

- t = the tangent altitude
- λ = the analysis wavelength
- FWHM = the full width at half maximum of the spectral filter
- Ω_{source} = the solid angle of the source
- A_{source} = the area of the source

Table 9. Angular dimensions and orientation of the sources used in OpticStudio to model the bright limb scene.

	Tilt about Y		
	-3.505°	0°	3.505°
0.95717°	4.995°x0.09572°	2.01°x0.09572°	4.995°x0.09572°
0.86146°	4.995°x0.09572°	2.01°x0.09572°	4.995°x0.09572°
0.76574°	4.995°x0.09572°	2.01°x0.09572°	4.995°x0.09572°
0.67002°	4.995°x0.09572°	2.01°x0.09572°	4.995°x0.09572°
-0.67002°	4.995°x0.09572°	2.01°x0.09572°	4.995°x0.09572°
-0.76574°	4.995°x0.09572°	2.01°x0.09572°	4.995°x0.09572°
-0.86146°	4.995°x0.09572°	2.01°x0.09572°	4.995°x0.09572°
-0.95717°	4.995°x0.09572°	2.01°x0.09572°	4.995°x0.09572°
-3.505°	12°x4.995°		

In FRED the bright limb is modelled with randomly distributed point sources. The infield is modelled with 8000 point sources. The distribution is shown in Figure 13. The same method is used for both left and right near out-of-field sources i.e. 8000 randomly distributed point sources for both sides. As the covered field is larger than the infield, the near out-of-field has a smaller sampling than the infield.

The radiant power of the sources is calculated as for the OpticStudio sources but as a point source doesn't have a solid angle, the solid angle of one detector pixel was used.

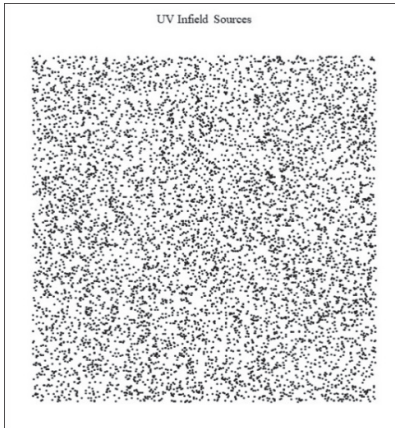


Figure 13. The distribution of the UV infield sources over the field of view in FRED

The approach of discrete random modelling was selected as a matter of convenience but further investigations have proven that the same approach than in OpticStudio can be used in FRED to simulate the scene as a continuous scene.

5. ANALYSES RESULTS

5.1 PSFs

Before performing a full stray light analysis, first some PSF's of point sources were compared.

The detector in the analysis has 501x501 pixels of 21 μ m. This corresponds to the field of view of the VIS channel, 2°x2°. In the UV channel it corresponds to 5.7°x5.7° or almost 3 times the infield FOV.

The X- and Y- cross section of the PSF at the central field point at 350nm and at 650nm in first order are shown in Figure 14. The PSF at 300nm is very similar to the PSF at 350nm. The OpticStudio and FRED results are quite similar. In the UV, the PSF's deviate slightly close to the specular peak, while in the VIS there is a small deviation at the edge of the detector. These differences are not explained by the differences between the ABg and Harvey-Shack models.

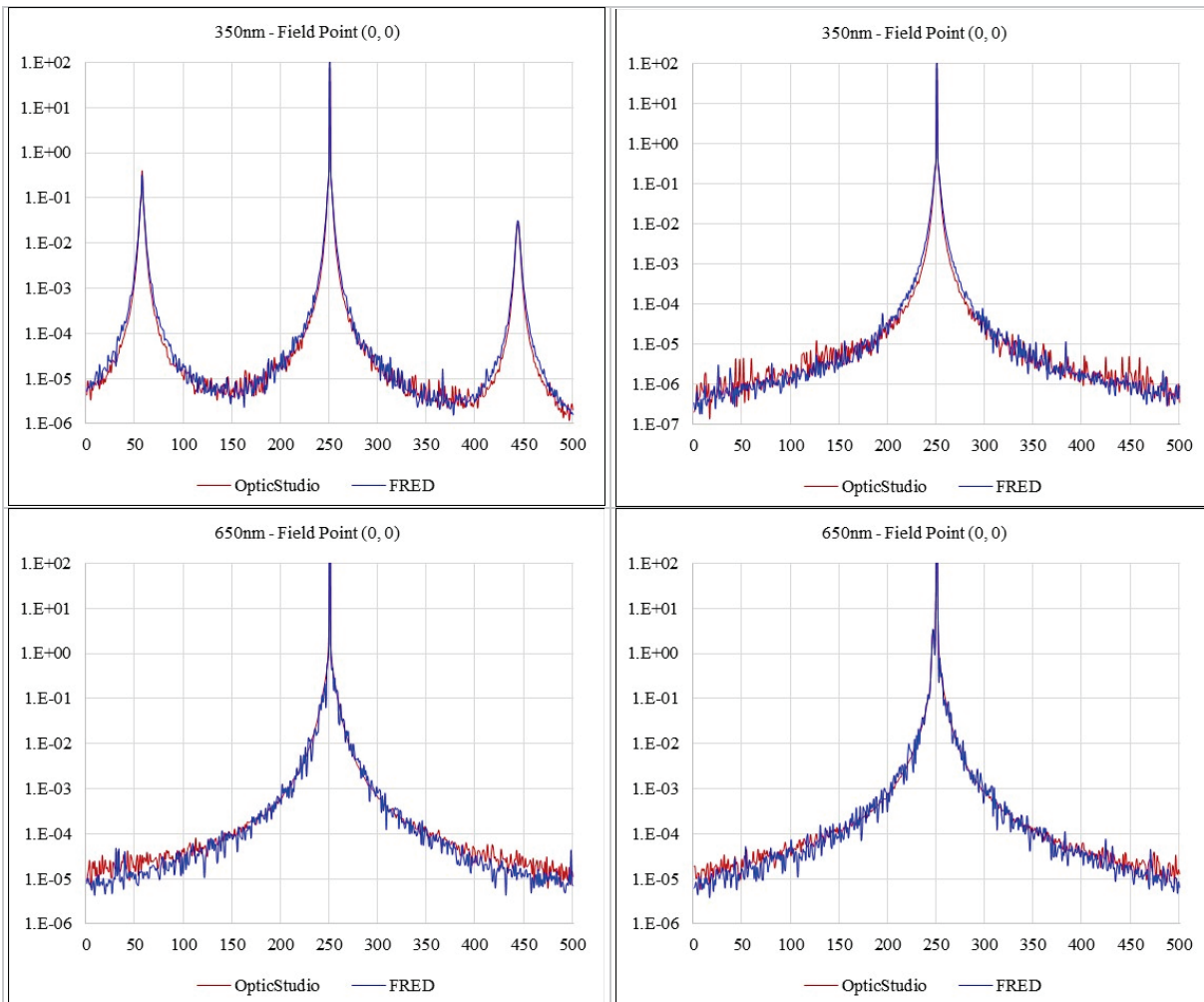


Figure 14. Cross Section in X (left) and Y (right) of the PSF at the central field point at 350nm (top) and 650nm (bottom)

In the VIS channel in zero order the differences are much larger. Figure 15 shows the \log_{10} of the PSF in W/mm^2 at 650nm in the zero order in FRED (left) and OpticStudio (right). From top to bottom an X-polarized source at the center field, a Y-polarized source at the center field, an X-polarized source at the corner field and a Y-polarized source at the corner field are shown. These are not really PSF's in the traditional sense because direct light from the zero order is blocked so all light reaching the detector has either scattered or ghosted.

In FRED the energy distribution are similar for X and Y-polarized sources, only the irradiance levels are different. In OpticStudio there are large differences depending on the polarization of the source. Other differences are:

- In OpticStudio sharply defined ghosts are present that are not seen in FRED.
- At the center field with the X-polarized source two central spots are visible in the OpticStudio PSF. These two spots originate from the ordinary and the extra-ordinary path in the AOTF crystal. The exact origin of the differences still has to be investigated but we expect that they are caused by the different modelling of the polarizers and the ancestry level in FRED that was set to 4.

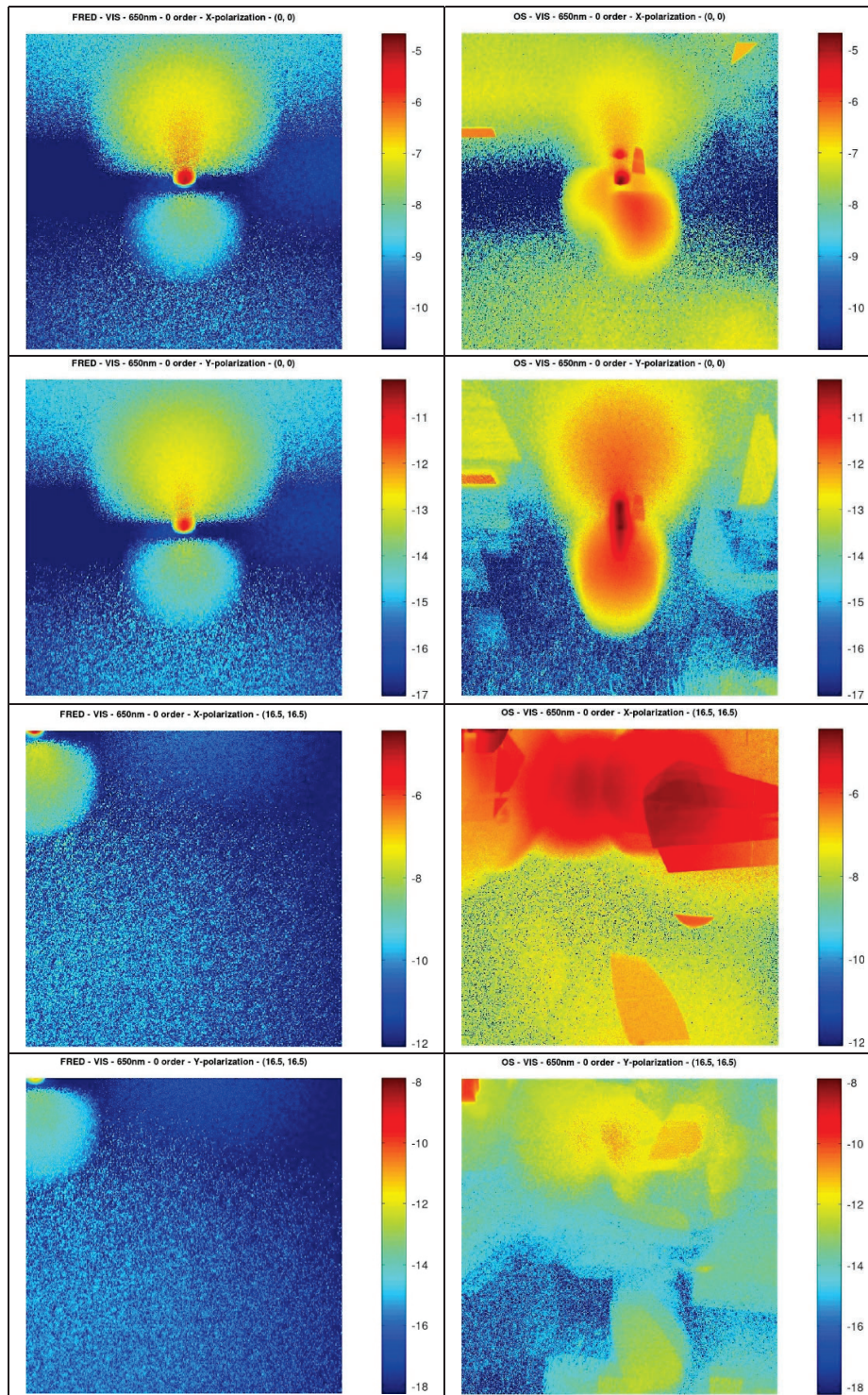


Figure 15. The log10 of the PSF at 650nm in W/mm^2 in the zero order in FRED (left) and OpticStudio (right) from top to bottom: X-polarized source center field, Y-polarized source center field, X-polarized source corner field, Y-polarized source corner field

5.2 UV channel Stray Light

The stray light in ALTIUS is calculated as the stray light to signal ratio. Signal is the irradiance on the detector when a simulation is performed without scattering or ghosting. Infield stray light is found by subtracting the signal from the irradiance on the detector when a simulation is done allowing scattering and ghosting with the infield sources only. Near out-of-field (NOoF) stray light is the irradiance on the detector when a simulation is done allowing scattering and ghosting with the out-of-field sources only.

$$SLRatio = \frac{((S+SL) - S_0)}{S_0} \tag{13}$$

The stray light to signal ratio is shown in Figure 16 for 300nm and 350nm, for both FRED and OpticStudio, as a function of the tangent altitude. For each tangent altitude, the average over the horizontal field of view and over a 5km vertical band is taken. A negative stray light to signal ratio originates when more light scatters away from the bright lower part of the scene than light scatters back in from other parts of the scene. The stray light to signal ratios are not very different between FRED and OpticStudio. The main difference is that the ratio increases much more rapidly at higher tangent altitudes in OpticStudio. Further study is needed to explain the differences.

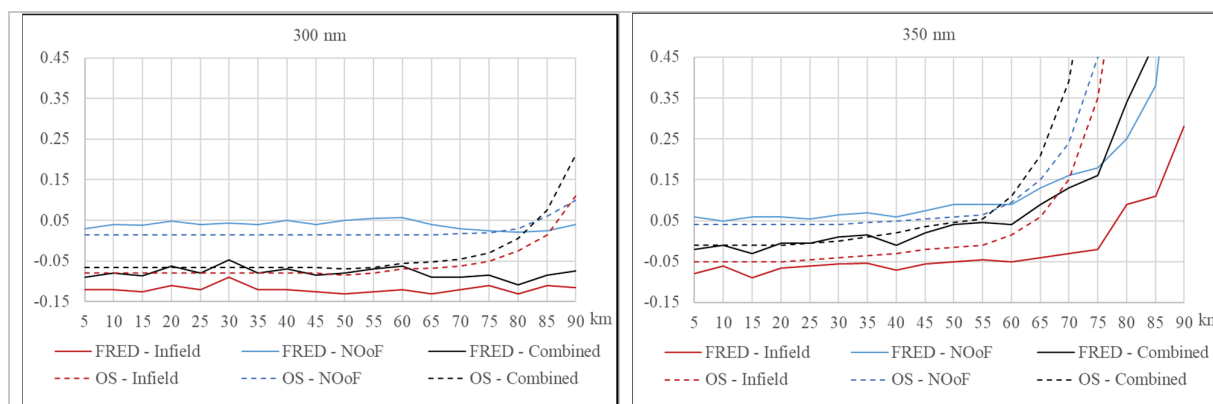


Figure 16. Stray light to signal ratio as a function of tangent altitude, for 300nm (left) and 350nm (right)

5.3 VIS channel Stray Light

The stray light calculations for the VIS channel are currently in progress. The stray light to signal ratio is calculated following the same conceptual approach as for the UV, with the additional complexity of the stray light created by the 0-th order.

6. CONCLUSIONS

The details and specificities of the stray light modelling of the ALTIUS UV and VIS channels have been presented for both OpticStudio and FRED optical softwares. It became apparent through the evaluation that both softwares are based on a different philosophy but also support a different mathematical background to model similar effects. As it could be seen OpticStudio showed to be more versatile and demonstrates a better capability to handle polarization effects than FRED while FRED has been showing much more powerful solving capabilities for “conventional” optics.

It was proven that despite modelling differences, workaround solutions could be identified in both models to represent ALTIUS optical elements and model performances. Obtained results were also shown to be very similar in terms of PSF

and infield stray light performances w.r.t a given scene. While scrutinizing more specific issues as the zero order stray light from an AOTF, which starts to get more closely related to illumination optics OpticStudio has been showing some interesting advantages in the capture of ghosts and the overall resulting illumination maps. Nevertheless, it shall be reported that the obtained results are not showing significant differences and results were using both softwares in a pretty good agreement.

The differences between softwares computations shall be, therefore, considered on the practical usage of these tools and workflow for the optical designer. From a computation standpoint both have been demonstrating a relatively equivalent computation time for a similar problem despite different capability to handle computer resources. OpticStudio appears a better tool to initiate the optical design and get a direct and quick understanding of the overall stray light performance of an optical system due to its embedded capabilities while FRED would be recommended in order to analyze more specifically certain stray light features and focus deeper on identified issues.

The developed stray light models described in this paper will be further improved during the course of the ALTIUS project by:

- Including as-built coating data
- Including tolerancing of the angular positioning of the Fabry-Perot cavities in the UV
- Further improving of the AOTF models
- Including updated scatter models

Specifically for the ALTIUS mission, these simulation tools will be used further in the project to support the development of the straylight reduction strategy at L1, generating more realistic data for correction algorithms robustness verification and anticipated worst case behavior. Finally, the ALTIUS stray light models will support the Instrument AIV activities through a correlation exercise with the results obtained from the Instrument flight model calibration campaign, in order to mitigate the need for extensive physical measurements at different wavelengths.

REFERENCES

- [1] M. Soman et al Non-linear responsivity characterisation of a CMOS Active Pixel Sensor for high resolution imaging of the Jovian system, JINST 10 (2015)
- [2] L. Montrone et al. Proc. SPIE 11151, Sensors, Systems, and Next-Generation Satellites XXIII, 111510S (2019)
- [3] N. Saillen et al. Technological innovation for the ALTIUS atmospheric limb sounding mission: step towards flight. This conference.
- [4] S. Valle Design and application of high performance Acousto-Optic Tunable Filters. (2017)
- [5] Michael G. Dittman "Contamination scatter functions for stray-light analysis", Proc. SPIE 4774, Optical System Contamination: Effects, Measurements, and Control VII, (2002);